Research Article | Vol. 12, No. 7 / 1 July 2021 / Biomedical Optics Express 4610
Biomedical Optics EXPRESS

Spectroscopy of excised skin patches exposed to THz and far-IR radiation

ALIREZA LAJEVARDIPOUR,[1,2,*] ZOLTAN VILAGOSH,[1,2] DOMINIQUE APPADOO,[3] JEFFREY DAVIS,[4] SAULIUS JUODKAZIS,[4,5] AND ANDREW WOOD[1,2]

[1]*Department of Health Sciences and Biostatistics, School of Health Sciences, Swinburne University of Technology, Hawthorn, Vic 3122, Australia*
[2]*Australian Centre for Electromagnetic Bioeffects Research, Swinburne University of Technology, Hawthorn, Vic 3122, Australia*
[3]*ANSTO-Australian Synchrotron, THz/Far-IR Beamline, Clayton, Vic 3168, Australia*
[4]*Optical Sciences Centre, School of Science, Swinburne University of Technology, Hawthorn, Vic 3122, Australia*
[5]*World Research Hub Initiative (WRHI), School of Materials and Chemical Technology, Tokyo Institute of Technology, 2-12-1, Ookayama, Meguro-ku, Tokyo 152-8550, Japan*
[*]*alajevardipour@swin.edu.au*

Abstract: Applications of far infrared (Far-IR) and terahertz (THz) radiation in areas such as healthcare and security are fast-growing. As a consequence, humans and the environment are becoming more exposed to mm-wave and Far-IR radiation than previously. We examined typical skin-care and sunscreen ingredients and propitiatory products with transmission FTIR, ATR-FTIR and THz-time domain spectroscopy (THz-TDS) methods using fresh and dehydrated toad and fresh human skin samples for their absorption properties in these frequency ranges. The skin hydration compounds glycerol and sorbitol have comparable absorption characteristics to physiological bulk water. Products containing these and similar hydrating compounds have significant Far-IR absorption characteristics. The sunscreen ingredients ZnO (20 micron), TiO_2 (mesh 325), and graphene platelet demonstrate a generally poor Far-IR absorbance, with TiO_2 displaying some frequency-specific absorption in the 3-6 THz and 12 THz regions. The Far-IR absorbance of proprietary sunscreens was, however, shown not to be significant. The absorption properties of melanin, collagen, bound water, and other constituents are significant in dehydrated skin samples but are not of the same order of importance as the hydrating agents examined.

© 2021 Optical Society of America under the terms of the OSA Open Access Publishing Agreement

1. Introduction

Big data storage and cloud computing in conjunction with IoT sensors and mobile devices have shaped an immense demand for data transfer requiring higher speeds and wider bandwidth in wireless communications. In response to this increasing demand, the utilising of higher frequency wireless communication is inevitable. 5G technology is presently emerging employing a range of frequencies all under 0.1 THz, but with higher frequencies already in prospect. Access to mm-wave and THz generators is becoming progressively easier. Applications of Far Infrared (IR) radiation in different technological areas like healthcare and security are fast growing. As a consequence, humans and the environment are more exposed to mm-wave and Far IR radiation than previously.

Infrared (IR) radiation extends from 700 nanometers (nm) to 1 millimeter (mm) which corresponds to a frequency range of approximately 430 THz (14000 cm^{-1}) down to 0.3 THz (10 cm^{-1}). Scientific and precautionary efforts have been made to produce international and national guidelines on limiting radiations in frequency ranges under 0.3 THz, Far-IR region, however, has received less attention. Due to the very low penetration depth of electromagnetic

#424267 https://doi.org/10.1364/BOE.424267
Journal © 2021 Received 4 Mar 2021; revised 14 May 2021; accepted 16 Jun 2021; published 1 Jul 2021

Biomedical Optics EXPRESS

field in the Far-IR region, scientific efforts on bioeffects of Far-IR radiation can be focused on superficial tissues, in particular the skin. It becomes vitally important to accurately predict the pattern of energy absorption of these forms of radiation, especially in the first few layers of cells on skin which are most likely to be near sources. The penetration depth of THz radiation in skin is around 300 µm at 0.5 THz [1], making it comparable to UVA penetration depth of 200 µm [2], but with a photon energy which is 1000 times less than that of UVA.

Several studies showed that Sun's IR-A may damage skin collagen content via an increase in matrix metalloproteinase-1 activity or formation of free radicals [3,4]. The International Commission on Non-Ionizing Radiation Protection (ICNIRP) guideline 2020 [5] and Brockow and *et. al.* [6] noted that the radiation above 0.3 THz can increase body core temperature beyond the 1°C operational adverse health effect threshold, however, there is still considerable uncertainty in specific physiological effects and tissue damage thresholds above 0.3 THz.

Around 50% solar energy consists of IR radiation. There is some evidence that sunscreens should also protect against Near-IR, in addition to protecting against UV [7,8]. Skin-care products often contain micro- or nano-sized formulation components, that can affect the amount of absorbed energy by the skin. It is reported that nano- and micro- particles do not penetrate into human skin beyond the superficial layer of the stratum corneum [9]. Thus, they remain in the boundary layer to face incoming radiation. Modern personal care products contain insoluble titanium dioxide (TiO_2), zinc oxide (ZnO) or nanoparticles (NP) [9]. Some other ingredients or nanoparticles are commonly used to affect skin hydration [10] where IR absorption is dominated by skin hydration level.

Here we address the absorption and absorbance profiles of toad and human skin patches exposed to Far IR radiation via different platforms. Toad skin was used due to ease of access and the ability to prepare dehydrated samples within ethical guidelines. There are some important differences between human and toad skin. Amphibians such as toads have a thin skin with epidermal and dermal layers similar to human skin (see Fig. 1). The epidermis layer includes melanophores that provide adaptable pigmentation patterns. Mammals, in contrast, have melanocytes in epidermis layers for coloration. The key pigment of both melanocytes and melanophores is black brownish melanin.

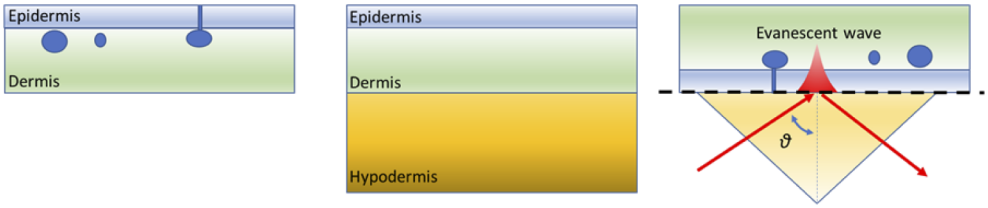


Fig. 1. Left) Typical amphibian skin with granular, mucosal glands and small mixed glands under epidermis layer. Middle) Overall layers of human skin. Right) Toad skin (epidermis down) on the ATR platform with diamond prism.

Although there is some evidence that melanin-containing structures provide some photo- and radio- frequency protection [11] in addition to the visible and UV spectrum [12], the extent of the melanin based absorption in the far IR frequency range is not well unknown. The hallmark of amphibian skin is the presence of various glands in dermis layer that perform vital physiological functions such as respiration [13,14]. However their contribution in absorption pattern is unknown.

Biomedical Optics EXPRESS

2. Results

We examined toad and human skin samples along with typical skin-care ingredients and products through transmission FTIR, ATR-FTIR and THz-Time Domain Spectroscopy (THz-TDS) methods.

2.1. Transmission FTIR study of skin

The transmission FTIR studies for fresh and previously dried toad skin over the range 26 –250 cm^{-1} (0.8 to 7.5 THz) are presented in Fig. 2. In transmission studies, the skin samples are located in an active vacuum chamber that remove the water content from fresh skin. This means that transmission studies are much more reliant on the properties of non-water elements of the skin in both the fresh and previously dried skin. In the graph of fresh toad skin (Fig. 2(A)), there are curves for various skin samples, with thicknesses ranging from 220 µm to 510 µm. Samples with 450 µm and 510 µm thicknesses are dark skin patches while 220 µm and 290 µm are pale ones.

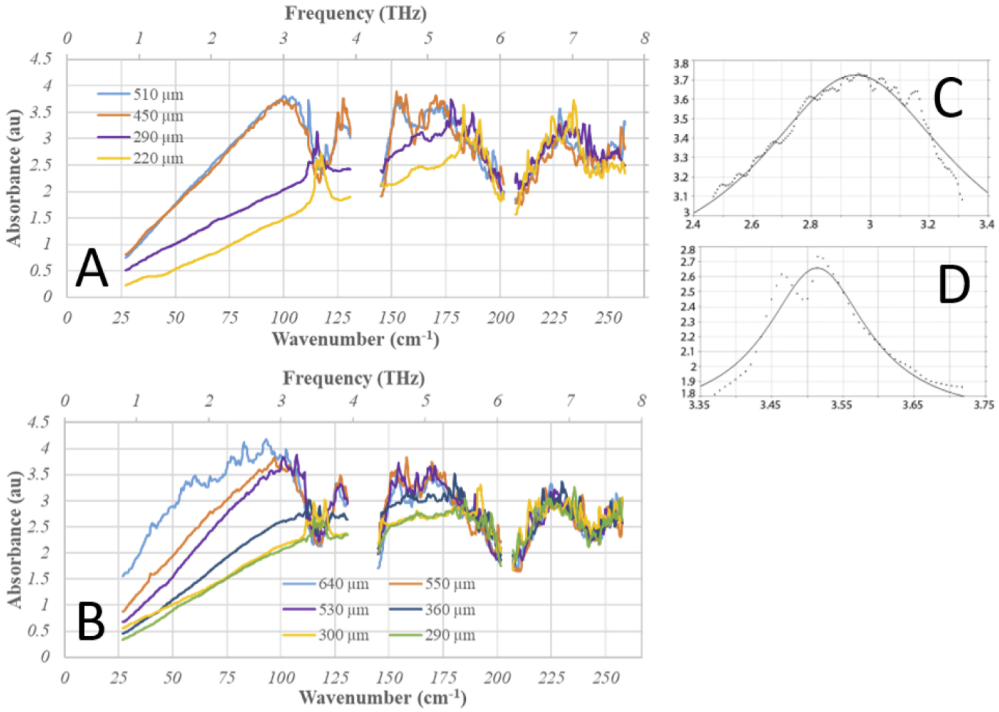


Fig. 2. (A) and (B) display the absorbance as a function of frequency for different fresh and dried toad skin samples, respectively. In both cases, absorbance curves separate in the range of lower than 175 cm^{-1}. The gaps in data are related to the lack sensitivity of the FTIR detector in specific ranges. (C) and (D) represent fitted Lorentzian functions for 450 µm curve at around 3 THz and 220 µm curve at around 3.5 THz, respectively.

In the > 175 cm^{-1} range, dark and pale absorbance curves overlap each other, however they are distinguishable below 175 cm^{-1}. In the case of 450 and 510 µm, the peaks of absorbances are located around 100 cm^{-1} which is equivalent to a wavelength of 100 µm. The peaks are located around 117 cm^{-1} (85 µm) for pale skin curves. There is a reduction of sensitivity with the detectors in the range of 100 to 150 cm^{-1}, which causes the apparent absorbance of all the samples to converge. This may be the cause of the disparity in the peak frequencies, as the peak

Biomedical Optics EXPRESS

reflectance values of the thick skin samples reaches a maximum that the detector can identify. The sensitivity improves at 150 to 175 cm^{-1}.

As a first approximation, we can treat the skin as a dielectric obeying the model of damped oscillators which its electric susceptibility is defined by the Lorentz model (Eq. (1)) [15]:

$$\chi(f) = \chi_0 + \frac{f_r^2}{(f_0^2 - f^2) - i\gamma f}, \tag{1}$$

where f_0 is the resonant frequency, γ represents the damping factor, f_r defines the strength of the resonance and χ_0 forms background susceptibility like Debye absorption [16] . One can obtain real and imaginary part of permittivity from complex susceptibility as equation set (2), assuming $\chi_0 = 0$:

$$\begin{aligned} \varepsilon'(f) &= 1 + \frac{f_r^2\,(f_0^2 - f^2)}{\left(f_0^2 - f^2\right)^2 + (\gamma f)^2}, \\ \varepsilon''(f) &= \frac{f_r^2 \gamma f}{\left(f_0^2 - f^2\right)^2 + (\gamma f)^2}. \end{aligned} \tag{2}$$

The (C) and (D) graphs in Fig. 2 depict fitted Lorentzian functions applied to data of fresh toad skin samples with thicknesses of 450 µm and 220 µm, respectively. By fitting imaginary part of susceptibility on the spectral distribution, one can obtain the Lorentz model parameters. The Table 1 displays fitting parameters of f_r, f_0, γ and R^2 for various thicknesses. R^2 is fitting coefficient of determination. From data in Table 1, it is evident that damping factor is directly related to sample thickness. Higher damping factor means higher absorption and broader peak.

Table 1. Parameters of fitting the imaginary part of electric susceptibility on spectral data of fresh toad skin only around 3 THz as shown in Figure 2(C). All frequencies are stated in THz unit.

Thickness (µm)	f_0	f_r	γ	R^2
510 ± 5	3.0	4.9	2.2	0.82
450 ± 5	3.0	4.9	2.2	0.86
290 ± 5	3.5	2.8	1.0	0.81
220 ± 5	3.5	2.6	0.08	0.83

Employing equation set (2) and fitted parameters reported in Table 1 lead us to obtain dielectric values of $\varepsilon' = 1.8$ and $\varepsilon'' = 2.03$ for 290 µm sample and $\varepsilon' = 0.55$ and $\varepsilon'' = 2.34$ for 450 µm sample at 3.3 THz (selected as an example but close to peaks). These values do not obey the trend reported by Chopra and *et. al.*[17] for thin epidermal plus dermal layers of human skin. However, their reported refractive index of less than 1 is not easily justifiable. On the other hand, each set of ε' and ε'' values reported here originated from the fitted curve of a specific peak with $R^2 \approx 0.8$. The limitation of fitting curve to only a specific peak rather than a whole graph impels a narrow validity range and an imposed uncertainty to both values.

The graph of dried toad skin samples in Fig. 2(B) includes five curves for skin thicknesses of 290 µm to 640 µm of which 530 to 640 µm samples are dark skin patches and 290 to 360 µm samples are pale ones. The overlap of absorbance curves in longer wavelengths and their separation in shorter wavelengths provides a facility to classify skin thicknesses by measuring absorption in the range of 25 – 175 cm^{-1}.

Biomedical Optics EXPRESS

2.2. THz time-domain spectroscopy of skin

We employed THz-TDS to examine effects of pigmentation level in the skin absorption. Figure 3 demonstrates absorption spectrum of THz radiation transmitted through different regions of a dried toad skin sample (with the thickness of 300 μm) where regions varied in pigmentation from fair to dark.

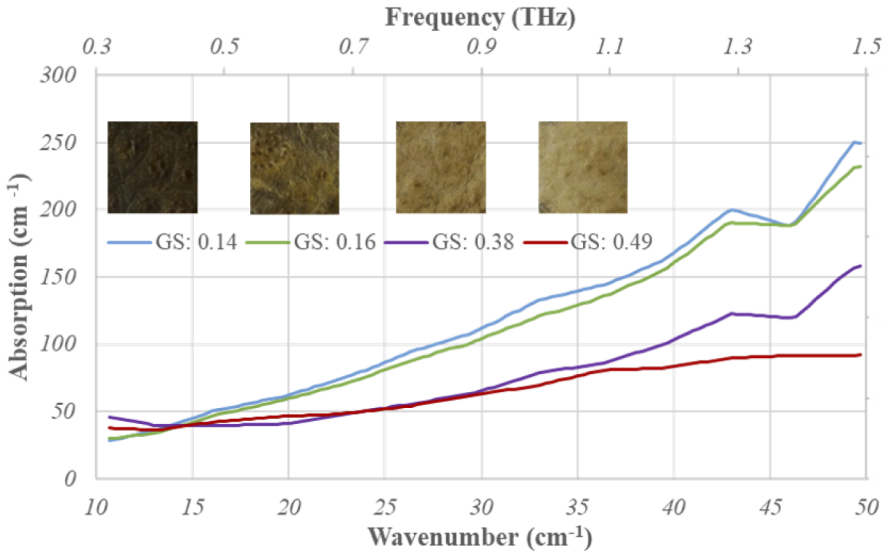


Fig. 3. The graph of absorption of toad skin patches with 4 different pigmentation (skin spot size of 2 by 2 mm). GS values represent pigmentation levels that have been calculated from RGB values of sample images. RGB images of sample spots are inserted as insets.

Here by employing an image-processing technique, we translated the pigmentation level of a skin spot as darkness of the spot in its colour image. The overall pigmentation level of skin spots is obtained from the Gray Scale (GS) value of the spot with the size of 2 by 2 mm (169 by 169 pixels). GS spans from 0 to 1 where 0 represents complete black colour and 1 signifies a pure white colour. To convert an RGB image to a single GS number, we first average R, G and B values of all pixels in the image then employ the conventional formula, Eq. (3), for converting averaged R, G and B values to a GS index, where R, G and B are the Red, Green and Blue pixel values, respectively.

$$GS = 0.29889\,R + 0.5870\,G + 0.1140\,B \tag{3}$$

To examine effects of skin hydration on absorption, we examined fresh toad skin sample through THz-TDS. Figure 4 displays changes of refractive index (A) and absorption (B) respect to hydration of fresh toad skin patches. The patch with thickness of 360 μm was exposed to air with an ambient temperature of 22 °C and with constant relative humidity of 40% (a typical condition for laser laboratory). The gradual dehydration occurs through steady evaporation of skin water with time. The absorption is very sensitive to skin hydration. The decrease of absorption is correlated with dehydration of skin patch in time where the lowest absorption was obtained when the skin became dry after 90 minutes exposure to air. Thus water content of skin governs its absorption in THz region. Figure 4(C) demonstrates a graph of absorption vs dehydration level at 1 THz where its data was extracted from Fig. 4(B).

Biomedical Optics EXPRESS

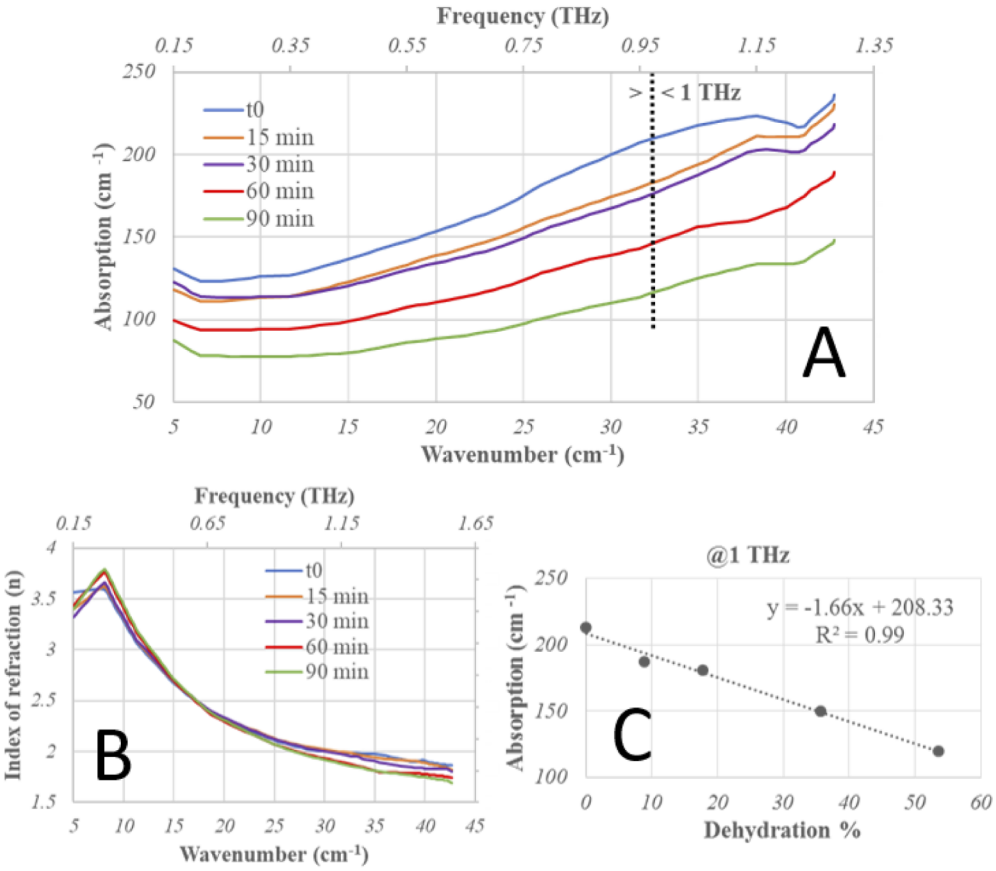


Fig. 4. (A) index of refraction, n, and (B) absorption of a fresh toad skin sample exposed to constant ambient temperature and humidity of laser lab. (C) displays a fitted line to absorption vs dehydration level at 1 THz.

2.3. ATR-FTIR study of skin

The ATR technique employs an evanescent wave to examine the surface layer of a sample. We used a FTIR spectrometer with an ATR platform to measure the absorbance of the epidermal layer of fresh toad skin. The skin samples include a dark thick patch and a fair thin patch. Results are depicted in Fig. 5 for two frequency regions much higher than the ranges depicted in Figs. 2–4.

Human skin patches (with typical thickness of 2 mm) are much thicker than toad skin samples which make them unsuitable for transmission study. Therefore, we employed ATR-FTIR spectroscopy to examine the absorbance of human skin. The graph in Fig. 6 demonstrates absorbance of fresh human skin and skin fat in mm-wave region. The graph displays a correlation between absorbance of skin and fat in low THz frequency range. It proves the higher penetration depth in low THz region. Human skin and fat share three peaks with tallest one at 346.9 GHz. It is important to note that the ATR setup with a diamond prism n = 2.39 at an angle of around 45°, can examine materials with n < 1.7 in attenuated total refection mode. Above n=1.7, the ATR setup becomes a reflectance/transmission apparatus. The evanescent wave generated by attenuated total refection is replaced by reflection at the surface and travelling wave propagation in the sample itself. Human skin is multilayered. The uppermost layer, the stratum corneum has a surface refractive index of 1.50 to 2.05 at 1.0 THz depending on hydration [18,19]. The refractive index at interface becomes a mixture of different refractive indices. The problem becomes more

Biomedical Optics EXPRESS

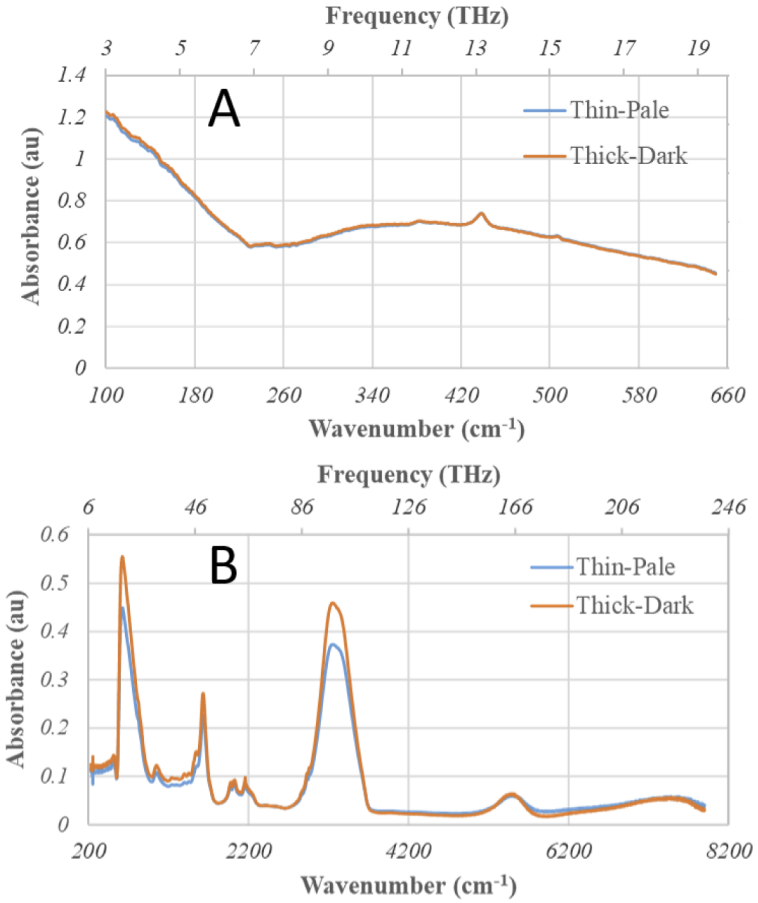


Fig. 5. ATR-FTIR spectroscopy of fresh toad skin in two different frequency ranges, with absorbance in arbitrary units. Two patches of fresh toad skin one thick and dark the other fair and thin.

complicated since the stratum corneum becomes more hydrated in the deeper layers [20]. It is the principal reason why a signal is obtained at some frequency lines as shown in Fig. 6.

2.4. Skin-care components and products

Sorbitol is a common ingredient in skin care products for preventing moisture loss from the skin. Figure 7(A) and 7(B) demonstrate the absorbance profile of water, glycerol and sorbitol in two different frequency regions through transmission-FTIR. They show transparency to mid-IR spectra, however some characteristic peaks are evident especially in 3200 cm^{-1}. In the Far-IR region, they show distinguishable absorbance patterns.

Nano- and micro- particles are ingredients in skin care product that demonstrate various absorbance profiles in ATR-FTIR measurements. Figure 8(A) and 8(B) display absorbance graphs of ZnO (20 micron), TiO_2 (mesh 325) and Graphene Platelet. Graphene Platelet shows absorbance in mid-IR, however TiO_2 demonstrates a better absorbance in far-IR. ZnO shows a very low absorption in low THz.

The sizes of the examined micro-particles are comparable to THz wavelengths. For example, the size of 20 microns is equivalent to the wavelength radiation in the frequency of 15 THz (or

Biomedical Optics EXPRESS

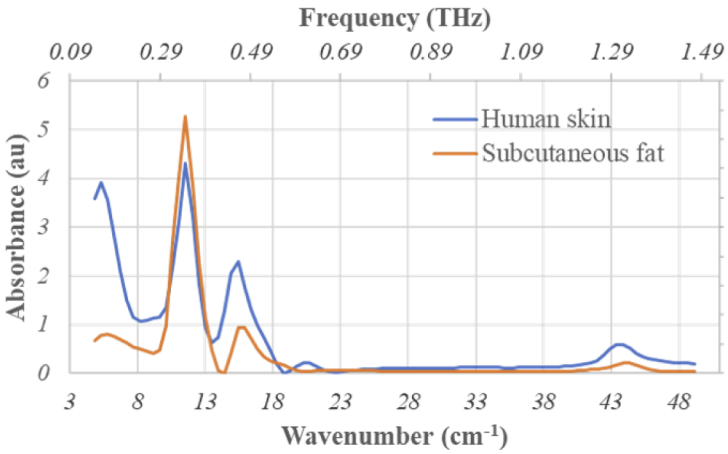


Fig. 6. ATR-FTIR spectroscopy of human skin and subcutaneous fat in mm-wave region with absorbance in arbitrary units..

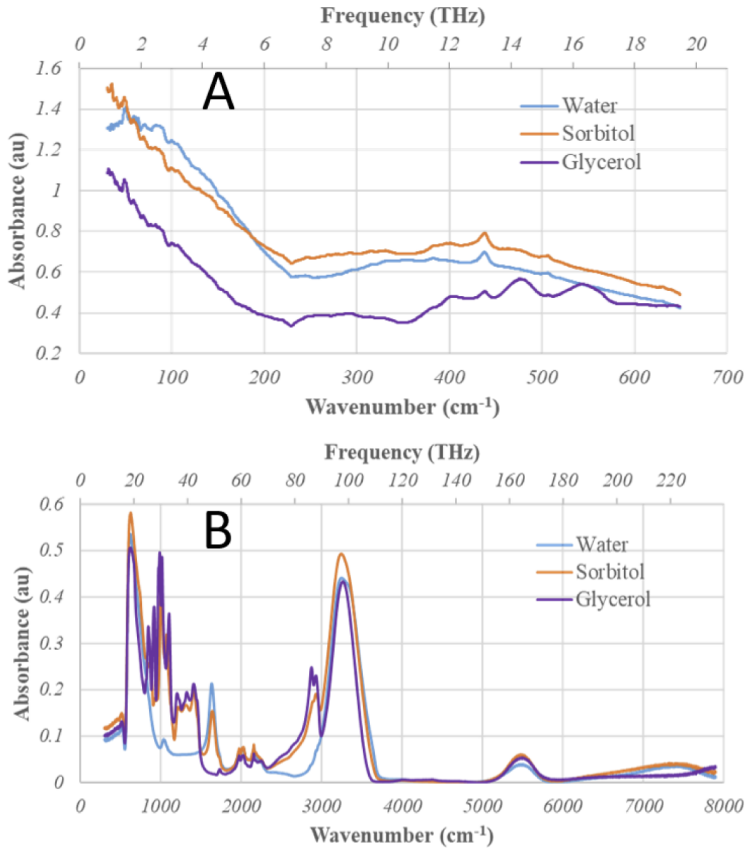


Fig. 7. Absorbance spectra (in arbitrary units) of distilled water, glycerol and sorbitol in two frequency regions. (A) Far-IR region (100 – 650 cm^{-1} or 3 –19.5 THz). (B) Mid-IR region (650 – 7800 cm^{-1} or 19.5 – 234 THz).

Biomedical Optics EXPRESS

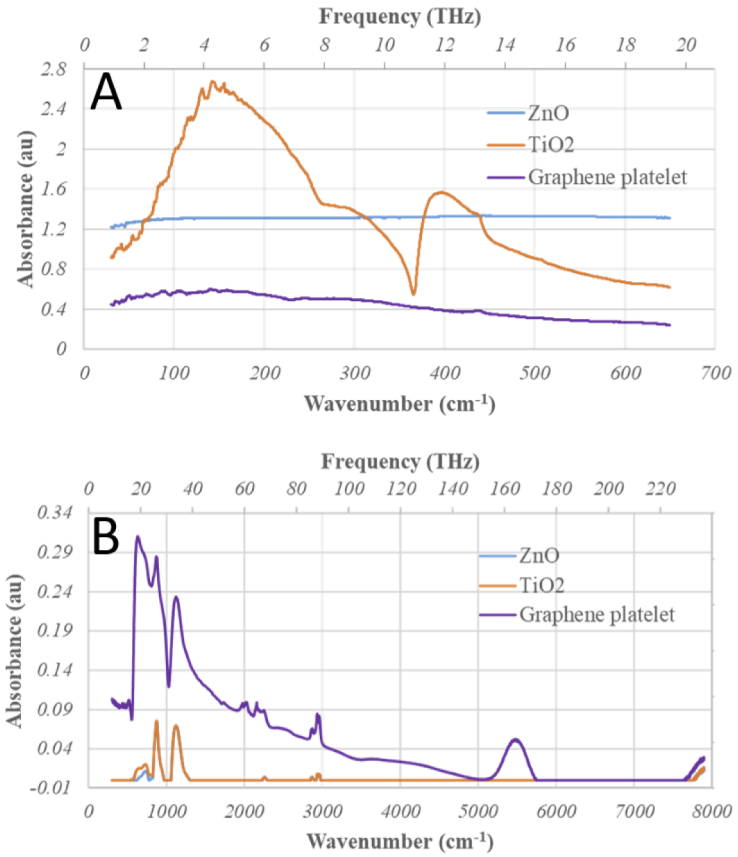


Fig. 8. Absorbance spectra (in arbitrary units) of micro-particles used in personal care production in IR frequency regions. (A) Far-IR region (100 – 650 cm^{-1} or 3 –19.5 THz). (B) Mid-IR region (650 – 7800 cm^{-1} or 19.5 – 234 THz).

500 cm^{-1}). It indicates that particle sizes are not negligible in the IR region and they will disturb absorption or scattering patterns.

To see overall absorbance profile of skin care products, we examined some commercial products available in Australian market using transmission-FTIR. Fig. 9 demonstrates absorbance spectra of some commercial personal-care products. They show a low level of absorbance in mid-IR range. The level of absorbances is almost the same from mid-IR to far IR. However, we can see an enhanced absorption for one product (BronZinc sunscreen) at around 380 cm^{-1} suggesting it is possible to have radiation-absorbing cosmetic preparation in the far-IR.

Figure 10 represents absorbance spectra of applied sunscreens and moisturisers on dried toad skin patches. The dried dark toad skin does not have significant absorption of sunscreens and moisturisers, however applied products impact absorption pattern in the far-IR range. As described in products descriptions, Neutrogena Hydro Boost sleeping mask is a skin hydrating product. Neutrogena is an oil-free moisturiser. SunSense product functions as sunscreen and moisturiser. The other products have only sunscreen properties.

Biomedical Optics EXPRESS

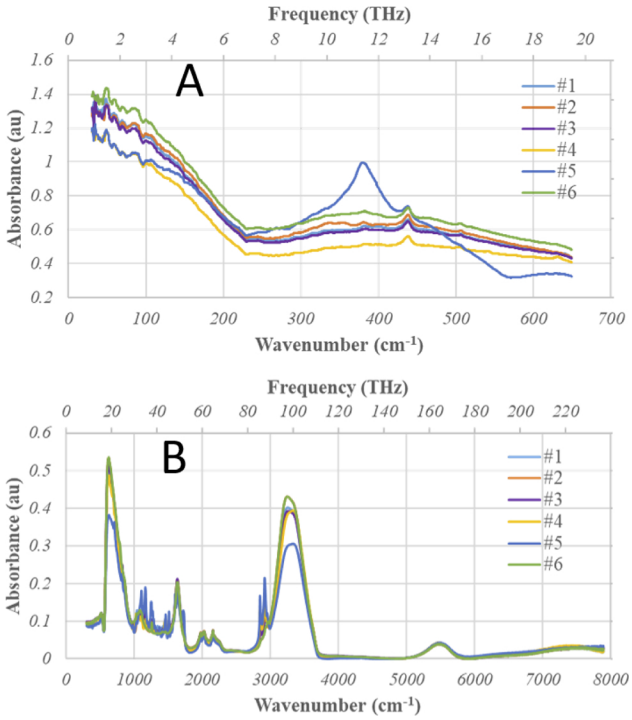


Fig. 9. Absorbance spectra (in arbitrary units) of commercial personal care products in two different frequency regions acquired through transmission-FTIR. The legends indicate #1: Neutrogena Oil-Free Moisture, #2: Nivea moisturising fluid with sun filter SPF 15, #3: Cancer Council everyday sunscreen, #4: BronZinc sunscreen SPF 30+, #5: SunSense ultra sunscreen SPF 50+, #6: Neutrogena HydroBoost sleeping mask. Left) The far-IR region (100 – 650 cm^{-1} or 3 –19.5 THz). Right) The mid-IR region (650 – 7800 cm^{-1} or 19.5 – 234 THz).

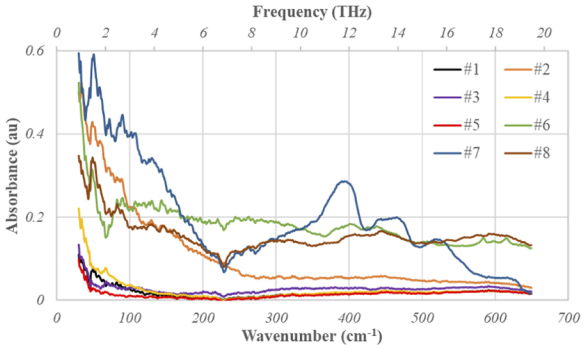


Fig. 10. The graph demonstrates effects of applied skincare products on absorbance spectra of completely dried dark toad skin patches through ATR-FTIR experiments. The legend enumerates #1: Dried dark toad skin sample without applying any product, #2: Neutrogena Oil-Free Moisture, #3: Nivea moisturising fluid with sun filter SPF 15, #4: Cancer Council everyday sunscreen, #5: BronZinc sunscreen SPF 30+, #6: SunSense ultra sunscreen SPF 50+, #7: Neutrogena HydroBoost sleeping mask, #8: Wetted dried toad skin. The absorbance profile of a dried toad skin patch wetted in water is added for comparison.

Biomedical Optics EXPRESS

3. Discussion and conclusion

In Fig. 2, the fresh and dried toad skin samples show a similar absorption pattern. Part of this similarity comes from the transmission FTIR setup where mounted samples are inserted in an actively evacuated chamber, which results in the dehydration of a wet specimen. The absorption pattern is the result of the skin becoming dehydrated, rather than any other mechanism.

Generally, scattering of incident radiation contributes to absorption measurement, however scattering dominates in high frequency ranges like UV regions where the wavelengths are much smaller than skin cells. By decreasing wavelength, the scattering moves from Mie scattering to Rayleigh scattering [21]. In the range of 250 – 500 cm^{-1} (40 – 20 μm) wavelengths are comparable with skin cell sizes of 20 to 40 μm. As reported in [21] in the epidermal layer, primary contributors to the scattering of incident wave are collagen fibres and water, however, at the longer wavelengths, water absorption becomes so significant as to dominate the absorption and scattering in the skin.

Fig. 3 introduces an absorption deference between high and low pigmented regions where dark regions (with high melanin density) absorb more. In various papers [12,21,22], it is noted that there is not much absorption by melanin below UV spectrum. However there are other reports available that note significant the absorption of melanin in THz range [23–26]. Bardon et al. [27] reported increasing ε'' with a stable ε' for a hydrated squid melanin over 0.45-1.00 THz.

In our studies, dark samples were generally thicker skin samples, however, Fig. 3, which displays absorption per length unit that is independent from skin thickness suggests a significant contribution of melanin in the absorption coefficient.

Although water content dominates radiation absorption, when bulk water is removed by dehydration, the displayed difference here needs to be interpreted using the absorption properties of melanin, with possible contribution by collagen, bound water and other constituents. The matter is confounded by the fact that thick toad skin patches have more mucosal glands beneath the epidermal layer [13] (as shown in Fig. 1). The mucosal glands may retain bulk water after dehydration and thus affect the absorption pattern.

Results of almost dried toad skin in Fig. 4 are in good agreement with reflection measurement of human forearm skin reported by Pickwell *et. al.* [28]. Using conversion equations of dielectric parameters (Eq. (4)), we can obtain $\varepsilon' = 2.9$ and $\varepsilon'' = 9.77 \times 10^{-5}$ at 1 THz. These values are quite different from dermal values reported by Sasaki et al. [29] as $\varepsilon' \approx 5$ and $\varepsilon'' \approx 2$. The value of $\varepsilon'' = 2$ corresponds to a conductivity of $\sigma = 2\pi f \varepsilon_0 \varepsilon'' = 111.2$ S/m at 1 THz which is almost equivalent to the conductivity of water [30] at that frequency.

$$\varepsilon' = n^2 - \left(\frac{c\alpha}{4\pi f}\right)^2, \qquad \varepsilon'' = \left(\frac{nc\alpha}{2\pi f}\right)^2 \tag{4}$$

In Fig. 4(C), a line is fitted on absorption versus percentage dehydration data which is calculated through well-known theory of evaporation from water surface in mg/min as Eq. (5) [31].

$$E = f(v)\, A\, (e^* - e)/60, \qquad f(v) = 25 + 19v \tag{5}$$

where $f(v)$ is an empirical function of air speed (v) in m/s, A is the surface area and e^* and e are saturated humidity ratio and humidity ratio, respectively. In the laser laboratory with controlled air conditions (temperature 21°C and humidity is 40%), values of e^* and e extracted from the Mollier diagram as 0.006 and 0.0153, respectively. For an air speed of 1 m/s and water surface area of 1 cm^2 the water evaporation rate is 0.625 mg/min. It is in good agreement with the

Biomedical Optics EXPRESS

evaporation rate for skin of human newborn in presence of air flowing reported in [32]. The toad skin is much thinner than adult human skin, but one can compare the thickness of toad skin with human newborn skin. The skin density of a newborn is 190 mg/cm^2 [33]. We assume the toad skin density equals to 150 mg/cm^2 that is composed of 70% water with water content of 105 mg/cm^2. From this value and the rate of evaporation (1.07 mg/min), we are able to estimate the dehydration percentage of skin patch after 15, 30, 60 and 90 minutes. The Fitted line in Fig. 4(C) indicates a linear relation between absorption and water loss in 1 THz. Results are well correlated with Maxwell-Wagner (MW) Eq. (6) for a binary mixture of water and skin components.

$$\varepsilon' = \varepsilon_s' \frac{(2\varepsilon_s' + \varepsilon_w') - 2\phi\,(\varepsilon_s' - \varepsilon_w')}{(2\varepsilon_s' + \varepsilon_w') + \phi\,(\varepsilon_s' - \varepsilon_w')} \tag{6}$$

where ε_s' is the permittivity of the dry skin, ε_w' is the permittivity of water and ϕ is the fraction of water in the skin. One can fit the MW equation with the line of $\varepsilon' = -1.66\phi + 3.7$ for $\varepsilon_s' = 3.76$ and $\varepsilon_w' = 2.1$ with the good accuracy of $R^2 = 0.995$.

Figure 2 demonstrates thickness depended peaks around 3-4 THz that are different from the water absorption spectrum in the same range. This indicates that the dielectric parameters in dried skin need to take account of non-bulk water components to explain absorption around 3-4 THz.

In the fresh toad skin ATR-FTIR spectroscopy at 3 to 250 THz, (Fig. 5), the absorbance of dark thick samples and fair thin samples overlap with the exception of a region around 8 THz and 90 THz. This implies that, in fresh skin, water retains its dominant position as the major absorber and that pigmentation does not significantly affect the absorbance throughout the 3 to 250 THz range.

ZnO and TiO_2 nano- and micro- particles are extensively used in personal-care product as UV absorbers. These ingredients, in their micro sizes, show notable absorption in the far-IR in relation to their size as demonstrated in Fig. 8.

Although sunscreen products can absorb UV light efficiently, our measurements demonstrated in Fig. 9 and 10 show that they are not very efficient in the IR range.

Moisturiser products, on the other hand, showed a degree of absorption in some specific frequencies. The mechanism is likely to be due to the adding of water or other polar compounds to the superficial layers of the skin. Majumdar and *et. al.* show that the hydration changes the physical and mechanical properties of stratum corneum [34].

Results indicate that hydration, whether naturally occurring or applied artificially, is effective at increasing the superficial skin absorption of THz and far IR radiation and thus reducing transmission to deeper skin layers. If specific protection was required, our experiments indicate that moisturiser products containing water or sorbitol are the most effective at reducing transmission. The bulk of radiation is absorbed on or above the dead stratum corneum and the superficial layers of the stratum spinosum.

4. Methods

In this study, we examined excised skin patches of cane toad and human arm to measure absorption of infrared and THz radiation. Moreover, we addressed the absorbance of skin care products and the related micro materials.

4.1. Toad skin preparation

Toad (Rhinella marinus) skin samples were obtained from animals euthanised by pithing. Patches (approximately 2 cm × 2 cm) were removed from dorsal (dark and thick) and ventral (light and thin) areas. These were placed into vials containing physiological saline and transported to the Australian synchrotron. The samples were used within hours of removal. Toad tissues are known to remain viable for several hours after excision.

Biomedical Optics EXPRESS

Dried toad skin patches were made by applying airflow around the hide in 22°C for a few hours. Then they were kept in the refrigerator.

4.2. Human skin preparation

Human skin samples were obtained from a local hospital. Patients for plastic surgery procedures had previously given informed consent to use some of the skin removed during surgery for synchrotron analysis. Samples were transported to the synchrotron in containers maintained at 4°C. Following analysis all tissues were disposed of according to the conditions for ethics approval.

4.3. Commercial samples

Some commercial skin-care products and ingredients available in the Australian market were randomly selected. There were no intention to select specific brand or product. They were chose based on their application.

- Sorbitol cosmetic grade moisturizer, ePharmacy Group Pty. Ltd., Australia,
- Glycerol with purity of >99.% all from Sigma-Aldrich Pty. Ltd., Australia
- Cancer Council everyday sunscreen SPF 30, Skin Health Pty Ltd, Australia,
- SunSense ultra sunscreen SPF 50+, EGO pharmaceuticals Pty. Ltd., Australia,
- BronZinc sunscreen SPF 30+, Church & Dwight Pty. Ltd., Australia,
- Nivea moisturising fluid with sun filter SPF 15, Beiersdorf Australia Ltd.,
- Neutrogena Oil-Free Moisture and HydroBoost sleeping mask, Johnson & Johnson pacific, New Zealand,
- Titanium Dioxide (TiO_2) 325 mesh powders with purity of 99.99%, Zinc Oxide (ZnO) 20 micron-powder with purity of 99.99% and Graphene Nanoplatelet 5 nm thickness and 30µm diameter with purity of 99.99% from NANOGRAFI Co. Ltd., Germany.

4.4. FTIR spectroscopy

The far-IR beamline is attached to a Bruker IFS 125/HR Fourier Transform (FTIR) spectrometer (Bremen, Germany). The spectrometer employs a Michelson interferometer with an optical path length of 942 cm. The spectrometer has different internal light sources like the Globar source that produces a beam in the range of 0.4 - 400 THz in addition to the main synchrotron source that covers the range of mm-waves to visible light. It is also equipped with an array of optical filters, detectors and beam-splitters offering selectable spectral regions from the THz to the mid-IR regions. Spectral resolution of 1 cm^{-1} was used for all experiments here. We chose a 6 µmulti-layer Mylar beamspliter and a Si: Bolometer detector with the detecting range of 10-370 cm^{-1} to the end of the beam path in our experiments.

The FTIR spectrometer is used to measure transmitted spectrum using both the direct transmission and ATR techniques through their dedicated sample holder platforms. In the direct transmission study, samples are mounted in the stage and inserted into the vacuum chamber in front of the beamline, while the ATR sample-platform does not need to be inserted into the vacuum chamber.

We employed the dedicated software (OPUS v8.0: Bruker Optik GmbH) to run the spectrometer for measurements and to export acquired data.

Biomedical Optics EXPRESS

The direct transmission mode measures transmittance percentage of a sample, where absorbance can be calculated through the mathematical relationship between transmittance and absorbance in Eq. (7).

$$|A(f)| = \log\left[1/\left(\frac{S_{sample}(f)}{S_{reference}(f)}\right)\right] \tag{7}$$

where S refers to the THz amplitude and $\frac{S_{sample}(f)}{S_{reference}(f)}$ is the relative transmission spectrum. Dividing sample spectrum by no-sample reference measurement eliminates the detector profile.

The attenuated total reflection (ATR) reflection studies utilised a diamond prism of refractive index 2.39 at an angle of around 45°. In ATR study, the penetration depth is low and depends on wavelength as given by Eq. (8).

$$\delta = \frac{\lambda_0}{2\pi\sqrt{(n_1 \sin\theta)^2 - n_2^2}} \tag{8}$$

where λ_0 is the wavelength in air, θ is indecent angle, n_1 and n_2 are refractive index of diamond prism and sample, respectively. For a typical refractive index of 1.5 the penetration depth is around 60 μm at 1 THz (33.33 cm^{-1} = 300 μm).

We did not apply any ATR correction here with respect to penetration depths. The penetration depth depends on the radiation wavelength and increases with decreasing frequency. Therefore, noncorrected ATR spectra have much stronger absorbance at higher frequencies. In this study, as we are solely comparing the ATR-FTIR spectra measured within this work, there is no need for performing any ATR corrections.

4.5. Sample mounting

For the transmission experiment in a vacuum chamber, two types of mounting were used regarding the physical state of samples. Skin patches were mounted between to metallic holder with a hole in centre for a ray transmission. The liquid samples were filled in a micro-chamber with transparent windows for the ray transmission.

ATR experiments were at room temperature and humidity. All samples were located on top of a diamond crystal and a sufficient pressure to remove any air at interface between diamond and sample, since any confined air between a sample and the ATR crystal would result in a weak signal.

4.6. THz time-domain spectroscopy

The details of the THz pulse generation and detection have been described previously [35]. Briefly, near single cycle THz pulses are generated by focussing a near-IR femtosecond laser pulse into a $LiNbO_3$ crystal using a tilted pulse front scheme [36,37]. The laser source is a 1 kHz Ti:Sa amplified laser emitting 100 fs long pulses with 420 μJ of energy, central wavelength 790 nm, bandwidth of 20 nm, and FWHM diameter of 4 mm. T The generated THz beam is focused onto the sample position, with a spot size, estimated with an iris, to be 2 mm FWHM, giving a peak field of ≈ 40 kV/cm. The transmitted THz is then recollimated and focused again onto a ZnSe crystal for the detection via electro-optical sampling, using a small amount of the 800 nm pulses as the sampling beam, which is picked off before the THz generation. The experimental setup is shown in Fig. 11.

Each THz time-domain trace is obtained by delaying the sampling beam by steps of 0.1 ps over a range of 14 ps. A trace takes less than 2 minutes. The frequency resolution is hence ~0.07 THz with a frequency cut-off of 2 THz.

The transmission of the pulsed electric fields is measured both through the empty sample holder, which we refer to as “air”, and with the mounted skin sample.

Biomedical Optics EXPRESS

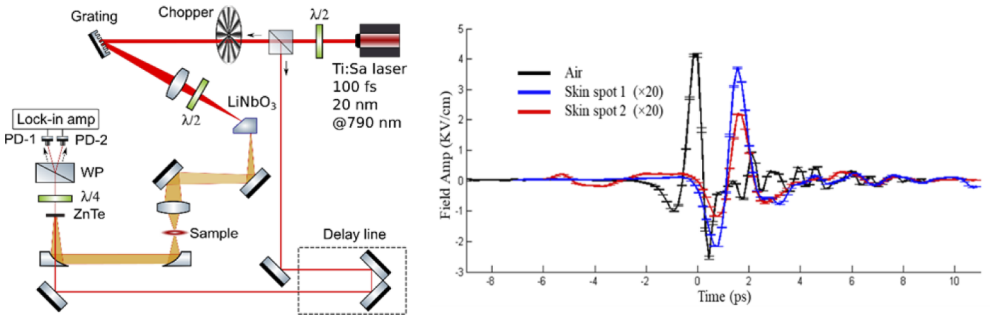


Fig. 11. Left) The optical diagram of our THz-TDS setup. Right) Time evolution of the pulse-resolved THz peak transmitted through air (reference- black curve) and two spots of a toad skin patch (spot 1- blue line, spot 2- red line). The skin transmitted pulses are multiplied by 20 for display purpose. Note that the centre of signal is shifted due to the delay applied upon transmission through samples.

The optical properties of the investigated samples are calculated by only considering the first transmission Fresnel coefficient of the skin sample and of the air reference. The time-domain data is Fourier transformed (FT) to give the magnitude and phase of the frequency-resolved transmitted THz field. By comparing the difference between the THz field measured through the sample and through air, the index of refraction (n) and absorption coefficient (α) for the sample are calculated through equation set (9).

$$\begin{aligned} \varphi &= \varphi_s - \varphi_{\text{ref}} \\ n(f) &= 1 + \frac{c\varphi}{2\pi f d}, \\ \alpha &= \frac{-20}{d} \ln\left(\frac{(1+n)^2}{4n} R\right) \text{cm}^{-1} \end{aligned} \tag{9}$$

where φ is the phase difference of Fourier Transformed (FT) transmitted field through sample (s) and air (ref), R is the ratio of the FT magnitudes, c is the speed of light, d is the sample thickness (in mm), and f represents frequency.

Uncertainties in the time-domain THz field detected are determined as the standard deviation of repeated measurements with the maximum error of ±3%. This error is propagated through the Fourier transforms and calculations of α and n or equivalently of ε' and ε''.

Funding. National Health and Medical Research Council (1042464); Australian Nuclear Science and Technology Organisation (15215, 15398); Australian Research Council (DP190103284).

Acknowledgements. This research partially funded by the National Health and Medical Research Council (Grant # 1042464) and was undertaken under grant numbers of 15215 and 15398 in the THz/Far-IR beamline at the Australian Synchrotron, part of ANSTO. We wish to acknowledge the partial contribution of Australian Research Council Discovery Project Grant (DP190103284) in this work.

We are grateful for assistance of scientific support Officer, Ms Ruth Plathe, at the Australian Synchrotron. We truly appreciate cooperation of Doctor Frank Bruscino-Raiola from plastic, hand & faciomaxillary surgery unit at Alfred hospital for providing human skin sample.

It is important to recognise Swinburne lab technicians, Christopher Anthony and Karl Hedger, for assisting us with preparing toad skin samples. We also appreciate technical assistance of Dr. Ashkan Roozbeh in THz-TDS lab.

The procedure for obtaining human skin samples was approved by the Swinburne Human Research Ethics Committee (2018/085) under ethic clearance of Alfred Health HREC Ref. 619/17. The procedure for obtaining the toad skin samples was also approved by the Swinburne University Animal Ethics Committee (SAEC 2019/01).

Disclosures. The authors declare no conflicts of interest and no competing financial interest.

A.L. and A.W. conceived the experiments, A.L., Z.V. and A.R. conducted the experiments, A.L. analysed experimental data, A.L, Z.V., D.A., S.J., J.D. and A.W. contributed in the result discussion, A.L. prepared the manuscript. All authors reviewed the manuscript.

Biomedical Optics EXPRESS

Data availability. Data underlying the results presented in this paper are not publicly available at this time but may be obtained from the authors upon request.

References

1. B. You, C.-Y. Chen, C.-P. Yu, P.-H. Wang, and J.-Y. Lu, "Frequency-dependent skin penetration depth of terahertz radiation determined by water sorption-desorption," Opt. Express **26**(18), 22709–22721 (2018).
2. M. Meinhardt, R. Krebs, A. Anders, U. Heinrich, and H. Tronnier, "Wavelength-dependent penetration depths of ultraviolet radiation in human skin," J. Biomed. Opt. **13**(4), 044030 (2008).
3. M. E. Darvin, S. F. Haag, J. Lademann, L. Zastrow, W. Sterry, and M. C. Meinke, "Formation of free radicals in human skin during irradiation with infrared light," J. Invest. Dermatol. **130**(2), 629–631 (2010).
4. C. Calles, M. Schneider, F. Macaluso, T. Benesova, J. Krutmann, and P. Schroeder, "Infrared a radiation influences the skin fibroblast transcriptome: mechanisms and consequences," J. Invest. Dermatol. **130**(6), 1524–1536 (2010).
5. ICNIRP, "Guidelines for limiting exposure to electromagnetic fields (100 khz to 300 ghz)," Heal. Phys. **118**(5), 483–524 (2020).
6. T. Brockow, A. Wagner, A. Franke, M. Offenbächer, and K. L. Resch, "A randomized controlled trial on the effectiveness of mild water-filtered near infrared whole-body hyperthermia as an adjunct to a standard multimodal rehabilitation in the treatment of fibromyalgia," The Clin. journal of pain **23**(1), 67–75 (2007).
7. D. Barolet, F. Christiaens, and M. R. Hamblin, "Infrared and skin: friend or foe," J. photochemistry photobiology. B, Biol. **155**, 78–85 (2016).
8. Y. Tanaka, "Impact of near-infrared radiation in dermatology," World J. Dermatol. **1**(3), 30 (2012).
9. G. J. Nohynek and E. K. Dufour, "Nano-sized cosmetic formulations or solid nanoparticles in sunscreens: a risk to human health?" Arch. Toxicol. **86**(7), 1063–1075 (2012).
10. S. A. Wissing and R. H. Müller, "The influence of solid lipid nanoparticles on skin hydration and viscoelasticity – in vivo study," Eur. J. Pharm. Biopharm. **56**(1), 67–72 (2003).
11. E. S. Pshennikova and A. S. Voronina, "Melanophores inside frogs," Int. Lett. Nat. Sci. **71**, 1–9 (2018).
12. G. Zonios, J. Bykowski, and N. Kollias, "Skin melanin, hemoglobin, and light scattering properties can be quantitatively assessed in vivo using diffuse reflectance spectroscopy," J. Invest. Dermatol. **117**(6), 1452–1457 (2001).
13. J. F. A. Varga, M. P. Bui-Marinos, and B. A. Katzenback, "Frog skin innate immune defences: Sensing and surviving pathogens," Front. Immunol. **9**, 202 (2019).
14. M. L. Ponssa, J. S. Barrionuevo, F. Pucci Alcaide, and A. Pucci Alcaide, "Morphometric variations in the skin layers of frogs: An exploration into their relation with ecological parameters in leptodactylus (anura, leptodactylidae), with an emphasis on the eberth-kastschenko layer," Anat. Rec. **300**(10), 1895–1909 (2017).
15. R. J. Churchill, "Absorption and spatial dispersion in electromagnetic susceptibility models," Phd thesis, University of Exeter, UK (2017).
16. A. Lajevardipour, A. W. Wood, R. L. McIntosh, and S. Iskra, "Estimation of dielectric values for tissue water in the terahertz range," Bioelectromagnetics **37**(8), 563–567 (2016).
17. N. Chopra, K. Yang, Q. H. Abbasi, K. A. Qaraqe, M. Philpott, and A. Alomainy, "Thz time-domain spectroscopy of human skin tissue for in-body nanonetworks," IEEE Trans. Terahertz Sci. Technol. **6**(6), 803–809 (2016).
18. K. I. Zaytsev, A. A. Gavdush, N. V. Chernomyrdin, and S. O. Yurchenko, "Highly accurate in vivo terahertz spectroscopy of healthy skin: Variation of refractive index and absorption coefficient along the human body," IEEE Trans. Terahertz Sci. Technol. **5**(5), 817–827 (2015).
19. S. Fan, B. Ung, E. P. J. Parrott, and E. Pickwell-MacPherson, "Gelatin embedding: a novel way to preserve biological samples for terahertz imaging and spectroscopy," Phys. Med. Biol. **60**(7), 2703–2713 (2015).
20. R. R. Warner, M. C. Myers, and D. A. Taylor, "Electron probe analysis of human skin: determination of the water concentration profile," J. Invest. Dermatol. **90**(2), 218–224 (1988).
21. M. J. Mendenhall, A. S. Nunez, and R. K. Martin, "Human skin detection in the visible and near infrared," Appl. Opt. **54**(35), 10559–10570 (2015).
22. R. R. Anderson and J. A. Parrish, "The optics of human skin," J. Invest. Dermatol. **77**(1), 13–19 (1981).
23. D. Lipscomb, I. Echchgadda, X. G. Peralta, and G. J. Wilmink, "Determination of the optical properties of melanin-pigmented human skin equivalents using terahertz time-domain spectroscopy," in *SPIE BiOS*, G. J. Wilmink and B. L. Ibey, eds. (SPIE, 2013), SPIE Proceedings, p. 85850F.
24. X. G. Peralta, D. Lipscomb, G. J. Wilmink, and I. Echchgadda, "Terahertz spectroscopy of human skin tissue models with different melanin content," Biomed. Opt. Express **10**(6), 2942–2955 (2019).
25. Z. Vilagosh, A. Lajevardipour, and A. Wood, "An empirical formula for temperature adjustment of complex permittivity of human skin in the terahertz frequencies," Bioelectromagnetics **40**(1), 74–79 (2019).
26. Z. Vilagosh, A. Lajevardipour, and A. W. Wood, "Computational phantom study of frozen melanoma imaging at 0.45 terahertz," Bioelectromagnetics **40**(2), 118–127 (2019).
27. T. Bardon, R. K. May, P. F. Taday, and M. Strlič, "Systematic study of terahertz time-domain spectra of historically informed black inks," The Analyst **138**(17), 4859–4869 (2013).
28. E. Pickwell, B. E. Cole, A. J. Fitzgerald, M. Pepper, and V. P. Wallace, "In vivo study of human skin using pulsed terahertz radiation," Phys. Med. Biol. **49**(9), 1595–1607 (2004).

Biomedical Optics EXPRESS

29. K. Sasaki, M. Mizuno, K. Wake, and S. Watanabe, "Measurement of the dielectric properties of the skin at frequencies from 0.5 ghz to 1 thz using several measurement systems," in *2015 40th International Conference on Infrared, Millimeter, and Terahertz waves (IRMMW-THz)*, (2015), pp. 1–2.
30. V. G. Artemov, A. A. Volkov, and N. N. Sysoev, "Conductivity of aqueous hcl, naoh and nacl solutions: Is water just a substrate?" Europhys. Lett. **109**(2), 26002 (2015).
31. "Engineering toolbox: Evaporation from water surface," https://www.engineeringtoolbox.com/evaporation-water-surface-d_690.html. Accessed: 2021-02-20.
32. I. H. Blank, "Factors which influence the water content of the stratum corneum," J. Invest. Dermatol. **18**(6), 433–440 (1952).
33. M. Leider, "On the weight of the skin**from the new york skin and cancer unit, department of dermatology and syphilology (marion b. sulzberger, m.d. director) and the post graduate medical school of the new york university-bellevue medical center," J. Invest. Dermatol. **12**(3), 187–191 (1949).
34. E. H. Mojumdar, Q. D. Pham, D. Topgaard, and E. Sparr, "Skin hydration: interplay between molecular dynamics, structure and water uptake in the stratum corneum," Sci. Rep. **7**(1), 15712 (2017).
35. F. Novelli, S. Ostovar Pour, J. Tollerud, A. Roozbeh, D. R. T. Appadoo, E. W. Blanch, and J. A. Davis, "Time-domain thz spectroscopy reveals coupled protein-hydration dielectric response in solutions of native and fibrils of human lysozyme," J. Phys. Chem. B **121**(18), 4810–4816 (2017).
36. H. Y. Hwang, S. Fleischer, N. C. Brandt, B. G. Perkins, M. Liu, K. Fan, A. Sternbach, X. Zhang, R. D. Averitt, and K. A. Nelson, "A review of non-linear terahertz spectroscopy with ultrashort tabletop-laser pulses," J. Mod. Opt. **62**(18), 1447–1479 (2015).
37. N. Nemoto, T. Higuchi, N. Kanda, K. Konishi, and M. Kuwata-Gonokami, "Highly precise and accurate terahertz polarization measurements based on electro-optic sampling with polarization modulation of probe pulses," Opt. Express **22**(15), 17915–17929 (2014).

137.157.8.210 2025-10-26 17:46:56